Published in the Proceedings of the 16th International Aluminum Alloys Conference (ICAA16) 2018
ISBN: 978-1-926872-41-4
by the Canadian Institute of Mining, Metallurgy & Petroleum

POTENTIAL FOR IN-SITU SOLUTIONISATION OF WIRE AND ARC ADDITIVE MANUFACTURED (WAAM) 2XXX ALUMINIUM ALLOYS

*J. Fixter[1], E. Eimer[2], Z. Pinter[2], B. Chehab[3], and P. Prangnell[1]

[1]*School of Materials*
University of Manchester, Manchester, UK
*(*Corresponding author: joseph.fixter@postgrad.manchester.ac.uk)*

[2]*Cranfield University, Milton Keynes, UK*

[3]*Constellium, Parc Economique Centr'Alp*
725 rue Aristide Bergès - BP 27
38341 Voreppe Cedex, France

ABSTRACT

High deposition rate Wire and Arc Additive Manufacture (WAAM) can provide benefits to the aerospace industry, including a reduction in lead time, reduced material waste and, through higher solidification rates, refinement of the as-built microstructure relative to a cast material. However, candidate 2xxx series high strength alloys for this process normally require a solution treatment, which is problematic for large near-net-shape components, and age hardening to achieve maximum mechanical properties. With each layer being subject to multiple thermal cycles, exploiting the thermal conditions in the WAAM process to avoid post-build solution treatment is therefore of interest. A solutionisation model has been developed for the WAAM process, based on diffusion controlled dissolution using DICTRA, which was validated through thermal simulations combined with 2D and 3D image analysis. The model has subsequently been used to simulate the solutionisation behavior during a typical WAAM thermal cycle and to explore what could theoretically be achieved by, for example, refining the starting microstructure.

KEYWORDS

Additive manufacturing, CALPHAD, DICTRA, Solutionisation, Dissolution, Al_2Cu

INTRODUCTION

There is currently great interest in exploiting additive manufacturing (AM) in the aerospace sector due to several benefits it can potentially provide; including reduced material waste, shorter product lead times and greater design freedom (Herzog, Seyda, Wycisk, & Emmelmann, 2016). However, with aluminium alloys the material properties obtained are generally inferior to those of conventional high-strength wrought products; therefore more research is required to explore the potential for exploiting the unique process conditions in AM to improve the as-deposited microstructure. A range of AM techniques are now available (Debroy et al., 2018), which differ in terms of the feedstock type and power source and it is necessary to match the appropriate technology to a particular application. This generally requires a compromise between the build rate and shape resolution. Wire and plasma-arc additive manufacturing involves using an electric arc to melt wire onto a substrate, and fabricates a part by building up overlapping layers of deposited weld beads (Addison et al., 2015; Williams et al., 2015). The benefits of this process over other AM methods are the much higher deposition rates (e.g. kg's/hour) achievable and lower capital equipment costs relative to powder bed techniques, which makes it suitable for large scale applications. However, limitations include a lower part complexity, lower solidification rates and a greater need for post-process machining (Frazier, 2014).

Aluminium alloys currently used for AM focus on the Al-Mg and Al-Si systems due to their good castability and low crack sensitivity (Bartkowiak, Ullrich, Frick, & Schmidt, 2011; Fiocchi, Tuissi, Bassani, & Biffi, 2017), but such materials are not suitable for the aerospace industry owing to their low mechanical performance. Of the conventional alloys used in aerospace, 7xxx series alloys are problematic in WAAM due to their tendency for hot cracking and zinc evaporation (Mukherjee, Zuback, De, & DebRoy, 2016). 2xxx series alloys, such as 2024, are thus of more interest due to their greater compatibility with the WAAM process and lower crack sensitivity (Pickin, Williams, Prangnell, Derry, & Lunt, 2013). However, to achieve high strength in such materials multiple heat treatment steps are normally required, including solution treatment to dissolve the eutectic phases formed on solidification so that their solute can be used for precipitation in subsequent ageing (Polmear, 1989). Unfortunately, solution treating large near-net-shape parts is problematic due to the risk of distortion and residual stresses on quenching (Collins, Brice, Samimi, Ghamarian, & Fraser, 2016). However, within the WAAM process there is potential to at least partially solution treat an alloy in-situ (during part fabrication) by exploiting the cyclic nature of the thermal history; i.e. by controlling the heating cycle experienced by the previously deposited layer when laying down the next track in the build sequence. This is also facilitated by the high solidification rates achieved in AM processes which produces a greatly refined dendritic solidification structure with much finer eutectic phases than seen in conventional DC casting (David & Vitek, 1989). In addition, in the WAAM process it is possible to further increase the level of solutionisation by using additional heat sources and exploiting in process deformation (e.g. layer rolling (Donoghue et al., 2016)) to accelerate the dissolution kinetics (Liu, Bai, Zhou, & Gu, 2011) .

In general, modelling solid state transformations in metals can be approached from two directions, using a sharp interface model (Vermolen, Vuik, Javierre, & Van Der Zwaag, 2005) or a phase field model (Chen, 2002). The phase field method describes the microstructure by modelling the interfaces as diffuse regions, which are controlled by a set of phase-field variables (Zhu, Wang, Zhou, Liu, & Chen, 2004). Typically, the disadvantages of the phase field method include a lack of obtainable parameter values, therefore requiring the energy function to be fitted rather than use physically justified values (Vermolen, Vuik, & van der Zwaag, 2003), and lengthy setup and computational times, not allowing for fast estimated solutions. However, the phase field approach can be extended to 2D and 3D morphologies to allow for complex shaped particles (Grafe, Böttger, Tiaden, & Fries, 2000). In contrast the sharp interface method involves modelling dissolution through the solutions of a multi-component Ficks diffusion equation (Durbin, 2005; Vermolen et al., 2003) and modelling the interface as sharp (i.e. no thickness), with regions either side allowing for mass transfer. The advantages include well documented thermodynamic and mobility data which allows for accurate 1D spatial modelling of multi-component systems, as well as fast computational times (Thornton, Ågren, & Voorhees, 2003; Vermolen et al., 2005). However, complex morphologies may not be accurately represented by this method, and it is difficult to expand it beyond symmetric 2D and 3D structures (Durbin, 2005).

The sharp interface model has been developed into the commercial software DICTRA (Thornton et al., 2003), which allows for quantitative predictions of diffusion based processes. However, owing to its greater speed and ease of operation this is the approach we have adopted in this paper. To determine if it is feasible to exploit in-situ solutionisation in AM with a high deposition rate processes like WAAM, a model has been developed to replicate the solutionisation behavior found in a simplified model alloy during the deposition steps. This has involved validating a DICTRA (Borgenstam, Höglund, Ågren, & Engström, 2000) -based dissolution analysis of the Al_2Cu phase in a 2319 alloy, and then using the model to predict the level of dissolution within typical WAAM thermal cycles. The model will be subsequently used to explore the level of solutionisation that could theoretically be achieved by using higher solidification rates, or incorporating additional heating cycles and a deformation step into the WAAM process. Some preliminary examples of this work are included in this paper.

EXPERIMENTAL METHOD

θ (Al_2Cu) phase dissolution modelling was performed with Thermocalc's diffusion package DICTRA, using the thermodynamic databases TCAL4 and mobility database MOBAL3. Initially, 1D planar and 2D cylindrical simplified geometries were modelled in order to determine which most reliably described the dissolving eutectic. A circular (cylindrical) geometry (2D) model was found to give adequate accuracy, when calibrated against experimental data (see Figure 2a). The models were set up using the measured initial θ volume fraction and used standard validated diffusion data for Cu in Al. The width of the θ particle was set to 1µm, with the cell size adjusted to achieve the desired initial volume fraction (vf = 0.06). This model was subsequently used to predict the level of solutionisation expected under standard WAAM conditions and explore the effect of varying the initial cell/particle size with a constant volume fraction (to replicate solidification rates). 2319 alloy WAAM samples produced by Cranfield University were used for the experiments, with solution heat treatments performed on the final deposited layer, which had undergone no subsequent in-process thermal cycle. To validate the model, small samples were rapidly heated in a salt bath for a variety of times before water quenching. The samples were then metallographically polished and imaged in an FEI Quanta 650 SEM. Multiple images from each sample were analyzed in Matlab using threshold imaging via Otsu's method to determine the eutectic particle sizes and volume fractions. A comparison was also made to 3D microstructural characterization of the eutectic phases using the Gatan™ 3View system in a FEI Quanta 250 SEM. Higher resolution images of matrix precipitation were taken with a FEI Magellan SEM.

Measurement of the standard WAAM thermal cycle was performed by pre building 10 layers using an AC-plasma TIG source. Thermocouples were then precisely inserted into the top layer before further layers were deposited. The wall was built with a wire feed speed (WFS) of 4.3 m/min, and a torch travel speed (TS) of 0.21 m/min. In order to more systematically investigate the effect of a more refined as-built microstructure, a copper wedge casting of the 2319 alloy was used to create a larger range of dendrite arm spacing's. The wedge was then sectioned and heat treated in the salt bath as explained above at 545°C.

RESULTS AND DISCUSSION

Figure 1a shows example of SEM images obtained of the eutectic phases in the as-built material and salt bath samples, solution treated at 545°C, along with the volume fractions measured as a function of time by image analysis. The initial θ volume fraction measurement is consistent with Scheil-Gulliver thermodynamic predictions (V_f = 0.06) based on the composition of the alloy used. The dissolution behavior follows the expected pattern (Hall & Haworth, 1970); in the rate is initially very high, but after ~ 300 sec drops substantially as the matrix becomes saturated in copper. The volume fraction measured at full solution treatment was slightly higher than equilibrium thermodynamic predictions for θ (V_f = 0.005) due to the image analysis technique being unable to distinguish between different types of phases (e.g. Fe rich intermetallics, etc.). In the context of the WAAM process, a dissolution time of 300 sec is clearly too long relative to a single thermal cycle, which is at close to peak temperature for the order of only 1–3 sec. However, because of the fine starting microstructure the WAAM deposit is 50% solutionised within the relatively short heat treatment time of ~15 sec, which may be achievable with repeated thermal cycling and this will be explored further below.

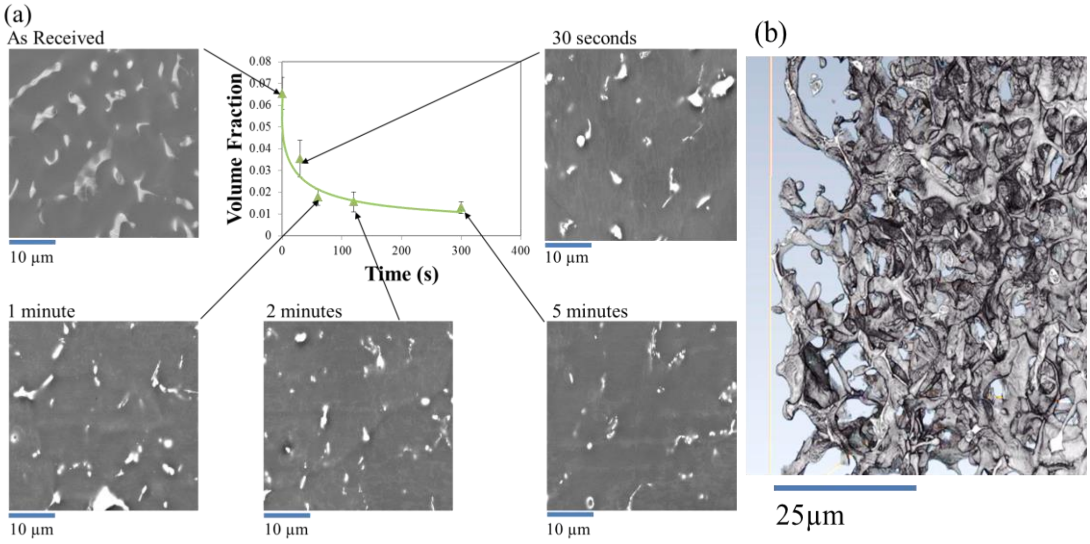

Figure 1. (a) Volume fraction analysis of samples solution treated in a salt bath for short times at 545 ºC. In (b) an example of the segmented eutectic structure is shown in 3D, using the 3View technique

Figure 2a highlights the effect of oversimplifying the geometry when modelling the dissolution of the Al_2Cu eutectic. It can be seen that the 2D model shows a much more rapid dissolution rate than the 1D model. This is also more consistent with the images in Figure 1a, which indicate that the eutectic phase distribution between the dendrite arms is closer to a cylindrical morphology than a continuous planar film, when sectioning is taken into account (Figure 1b), although as seem by the 3D segmentation the real morphology is extremely complicated and varies greatly locally. Figures 2b–2d further compare the measured volume fractions with the 2D model at different temperatures. These graphs indicate sufficient agreement with the experimental results to use the 2D representation to estimate the effect of thermal cycling and differing initial microstructures on the level of dissolution that can be expected in the WAAM process.

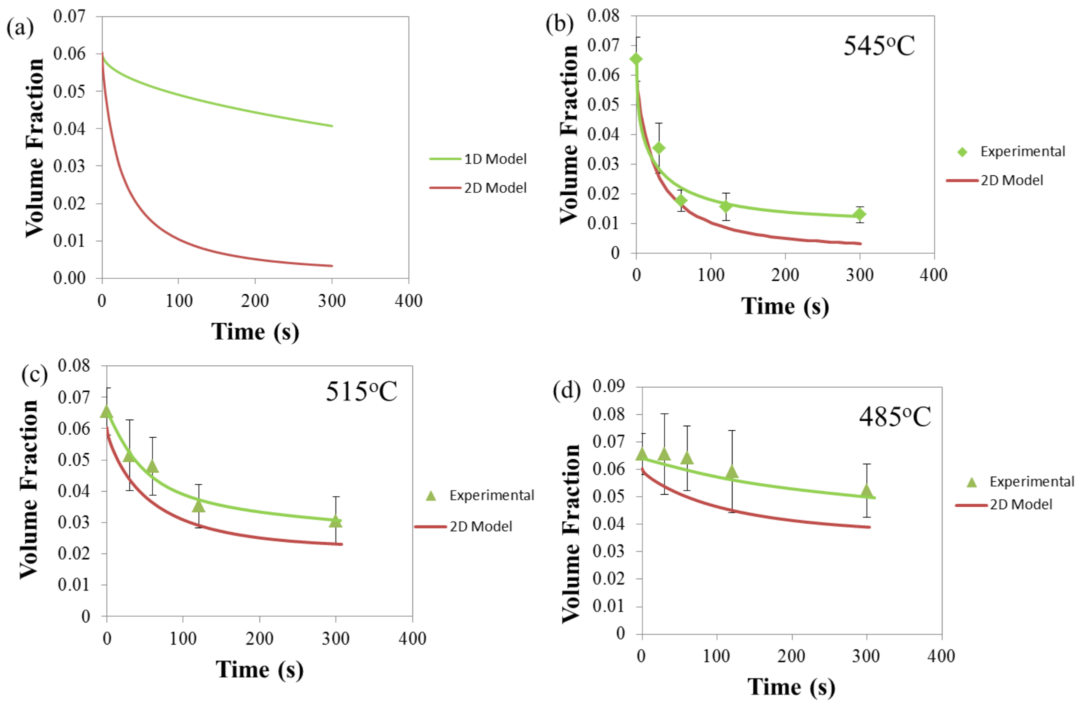

Figure 2. Comparisons between (a) the planar geometry and spherical geometry in the model and (b) – (d) the 2D model and experimental volume fraction data at different temperatures

Figure 3a shows a typical measured thermal cycle recorded for a single WAAM layer built using an AC-plasma TIG source. It can be seen that the temperature when the first layer was deposited is above the solidus temperature. However, for the subsequent 8 cycles the temperatures stayed below the solidus and above 500°C, allowing conditions compatible with solutionisation to occur. The predicted behavior of the primary eutectic θ volume fraction, using the thermal history from the second thermal cycle onwards, which was the first cycle below the melting point, is shown in Figure 3b where it is shown that the final θ level matches quite well with the volume fraction measured from the actual WAAM sample. Furthermore, it can be seen from Figure 3b (see insert) that as the peak temperature is reached in the second cycle, (i.e. the first re-solutionisation cycle) that the volume fraction of θ is predicted to substantially reduce by about 50%. However, on cooling the model predicts some re-growth at the end of this cycle. This results in a reduction in θ volume fractions to about 40%. With subsequent passes of the heat source it can also be noted that as the peak temperature drops, re-growth is predicted to win over solutionisation and the net volume fraction progressively increases. Therefore the level of solutionisation is actually worse than in the first reheating cycle. With the heat source and process parameters used, re-growth with lower peak temperatures can thus be seen to limit the amount of solutionisation that can be achieved. Overall the model thus suggests a substantial improvement could be made by using more controlled thermal management to control the decay in peak temperatures to maximize solutionisation (e.g. by applying a second heat source) and reducing the level of regrowth by increasing the rate of decay below ~ 530°C and increasing the cooling rate (e.g. through applying a coolant).

Another feature seen in Figure 3a is the buildup of heat as more layers are added as the time between repeated passes is not long enough for the heat to dissipate. Additional precipitation from solid solution would also therefore be expected to occur owing to increasing background temperature and thermal exposure below the measurement point, where a wide range of lower peak temperatures will be experienced in the build. This is seen in Figure 4a.

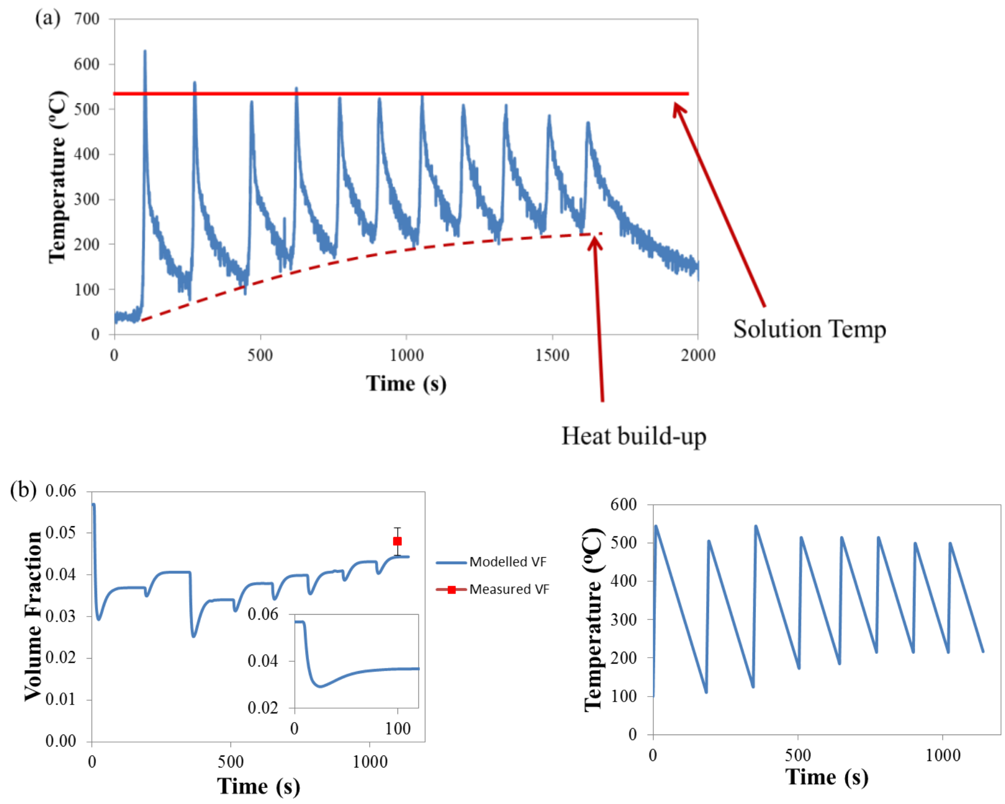

Figure 3. (a) Thermocouple data from WAAM of AA2319 deposited using AC-Plasma/TIG and (b) The corresponding predicted θ phase volume fraction, with the first cycle magnified as an insert to show the effects of dissolution and regrowth, along with the modelled temperature profile

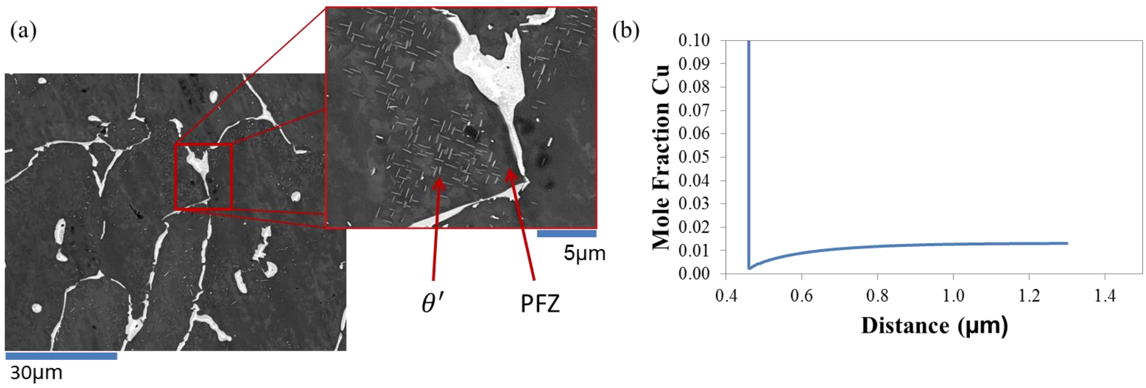

Figure 4. (a) SEM images showing precipitation of θ′ phase in the WAAM samples (b) model output showing the predicted copper depletion at the interface between the particle and the matrix

In Figure 4a, high resolution SEM images are provided highlighting precipitation occurring in the WAAM sample during the deposition of subsequent passes. It can be seen that θ′ is precipitated in the matrix near the cell boundary as there is a higher matrix concentration of copper generated by partial solutionisation on heating in previous passes. There is also a precipitate free zone (PFZ) present near the dendrite boundary, which, in the model, is predicted to be caused by regrowth of the θ eutectic phase upon cooling. This effect can be also seen in the diffusion model in Figure 4b, where after multiple cycles of heating and cooling, with rates determined from thermocouple data in Figure 3a, depletion of copper is seen next to the interface between the particle and the matrix on the same order as measured in Figure 4a (approximately 0.5 µm).

The effect of microstructure scaling has also been investigated, to determine if the dissolution rate could be increased with a more refined as-built microstructure (e.g. by increasing the cooling rate during deposition). It should be noted that in the solidification rate range of interest little Cu solute trapping occurs (Norman, Drazhner, & Prangnell, 1999) and this would be expected to have minimal effect on the model predictions, when a constant initial volume fraction is assumed. Figure 5a predicts how reducing the initial size of the eutectic film width (and hence dendrite cell spacing) can improve the dissolution rate. For example, by halving the initial particle size from 1 to 0.5 µm the time for 50% dissolution time drops by a factor of four. This is presumably because the diffusion distance is parabolically related to time and this significant increase in kinetics highlights the potential benefit of using an increased solidification rate to improve the response to solution treatment. Figure 5b shows experimental data obtained for solution treating samples with different initial eutectic particle/cell sizes from the wedge cast sample. The thickness of the eutectic films increased from 0.5–2 µm at the wedge tip (highest cooling rate) to 1–5 µm at the top of the mold. The results in Figure 5b show a corresponding increase in the dissolution rate at the tip of the wedge for short dissolution times, although this benefit reduces as saturation of the matrix is approached.

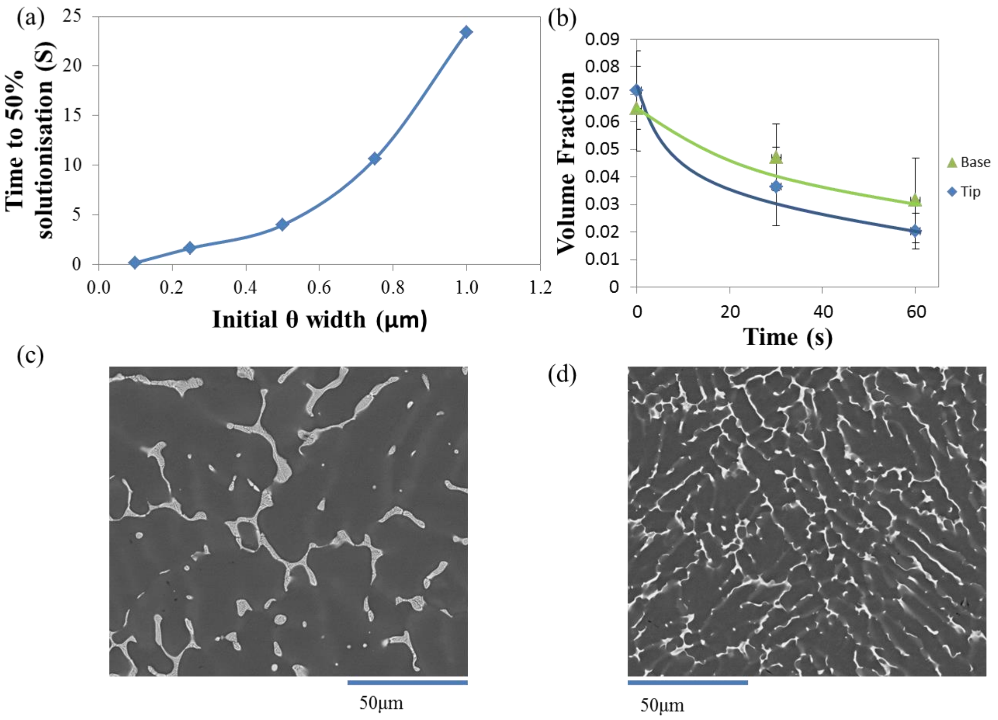

Figure 5. Predictions of the effect of scale on dissolution rate a) compared to b) experimental measurements of dissolution for the top and bottom of the wedge casting: c) and d) SEM images of the initial microstructure at the base and tip of the Cu chill wedge casting

CONCLUSIONS

A simplified model has been developed to predict the dissolution of the main eutectic constituent θ phase during WAAM deposition of the alloy AA2319, with a view to exploring the potential for optimizing the thermal management during AM to maximize the level of in-process solutionisation and thereby ultimately improve the mechanical properties of a deposited material. It has been shown that a 1D representation is not sufficient to predict the material response and an axisymmetric (circular disc) 2D representation is the simplest configuration required to obtain a reasonable prediction. The model has been successfully validated using experimental data. Predictions have been presented demonstrating how to improve the dissolution kinetics by, for example, refining the initial as-built microstructure. The model has also shown the importance of controlling the decay in peak temperature and increasing the cooling rate during subsequent deposition cycles to minimize the regrowth of the interdendritic eutectic phase and matrix precipitation. From this work it will be possible to explore options for improving the thermal management to maximize the amount of in-situ solutionisation; for example by optimizing the process parameters and the application of additional heating and cooling sources to each layer during the build.

ACKNOWLEDGMENTS

The authors acknowledge financial support from C-TEC, Constellium Technology Center, and EPSRC-UK through the CDT in Advanced Metallic Systems (EP/L016273/1) and are grateful to Rhys Thomas for assistance with high resolution imaging.

REFERENCES

Addison, A., Ding, J., Martina, F., Lockett, H., Williams, S., & Zhang, X. (2015). Manufacture of Complex Titanium Parts using Wire+Arc Additive Manufacture. *Titanium Europe 2015 Conference*, 14.

Bartkowiak, K., Ullrich, S., Frick, T., & Schmidt, M. (2011). New developments of laser processing aluminium alloys via additive manufacturing technique. *Physics Procedia*, *12*(PART 1), 393–401. https://doi.org/10.1016/j.phpro.2011.03.050

Borgenstam, A., Höglund, L., Ågren, J., & Engström, A. (2000). DICTRA, a tool for simulation of diffusional transformations in alloys. *Journal of Phase Equilibria*, *21*(3), 269–280. https://doi.org/10.1361/105497100770340057

Chen, L.-Q. (2002). Phase-Field models for microstructure evolution. *Annual Review of Materials Research*, *32*(1), 113–140. https://doi.org/10.1146/annurev.matsci.32.112001.132041

Collins, P. C., Brice, D. A., Samimi, P., Ghamarian, I., & Fraser, H. L. (2016). Microstructural Control of Additively Manufactured Metallic Materials. *Annual Review of Materials Research*, *46*(1), 63–91. https://doi.org/10.1146/annurev-matsci-070115-031816

David, S. a., & Vitek, J. M. (1989). Correlation between solidification parameters and weld microstructures. *International Materials Reviews*, *34*(5), 213–245. https://doi.org/10.1179/imr.1989.34.1.213

Debroy, T., Wei, H. L., Zuback, J. S., Mukherjee, T., Elmer, J. W., Milewski, J. O., … Zhang, W. (2018). Progress in Materials Science Additive manufacturing of metallic components – Process , structure and properties. *Progress in Materials Science*, *92*, 112–224. https://doi.org/10.1016/j.pmatsci.2017.10.001

Donoghue, J., Antonysamy, A. A., Martina, F., Colegrove, P. A., Williams, S. W., & Prangnell, P. B. (2016). The effectiveness of combining rolling deformation with wire-arc additive manufacture on β-Grain refinement and texture modification in Ti-6Al-4V. *Materials Characterization*, *114*, 103–114. https://doi.org/10.1016/j.matchar.2016.02.001

Durbin, T. L. (2005). Modeling dissolution in aluminium alloys. *Mechanical Engineering*, (March). Retrieved from http://citeseerx.ist.psu.edu/viewdoc/download?doi=10.1.1.491.2016&rep=rep1&type=pdf

Fiocchi, J., Tuissi, A., Bassani, P., & Biffi, C. A. (2017). Low temperature annealing dedicated to AlSi10Mg selective laser melting products. *Journal of Alloys and Compounds*, *695*, 3402–3409.

https://doi.org/10.1016/j.jallcom.2016.12.019

Frazier, W. E. (2014). Metal additive manufacturing: A review. *Journal of Materials Engineering and Performance*, *23*(6), 1917–1928. https://doi.org/10.1007/s11665-014-0958-z

Grafe, U., Böttger, B., Tiaden, J., & Fries, S. G. (2000). Coupling of multicomponent thermodynamic databases to a phase field model: application to solidification and solid state transformations of superalloys. *Scripta Materialia*, *42*(12), 1179–1186. https://doi.org/10.1016/S1359-6462(00)00355-9

Hall, M. G., & Haworth, C. W. (1970). Dissolution of θ phase in Al-5% Cu. *Acta Metallurgica*, *18*(3), 331–337. https://doi.org/10.1016/0001-6160(70)90148-3

Herzog, D., Seyda, V., Wycisk, E., & Emmelmann, C. (2016). Additive manufacturing of metals. *Acta Materialia*, *117*, 371–392. https://doi.org/10.1016/j.actamat.2016.07.019

Liu, Z., Bai, S., Zhou, X., & Gu, Y. (2011). On strain-induced dissolution of θ′ and θ particles in Al-Cu binary alloy during equal channel angular pressing. *Materials Science and Engineering A*, *528*(6), 2217–2222. https://doi.org/10.1016/j.msea.2010.12.060

Mukherjee, T., Zuback, J. S., De, A., & DebRoy, T. (2016). Printability of alloys for additive manufacturing. *Scientific Reports*, *6*(1), 19717. https://doi.org/10.1038/srep19717

Norman, A. F., Drazhner, V., & Prangnell, P. B. (1999). Effect of welding parameters on the solidification microstructure of autogenous TIG welds in an Al–Cu–Mg–Mn alloy. *Materials Science and Engineering: A*, *259*(1), 53–64. https://doi.org/10.1016/S0921-5093(98)00873-9

Pickin, C. G., Williams, S. W., Prangnell, P., Derry, C., & Lunt, M. (2013). Control of weld composition when arc welding high strength aluminium alloys using multiple filler wires. *Science and Technology of Welding and Joining*, *15*(6), 491–496. https://doi.org/10.1179/136217110X12785889549660

Polmear, I. . (1989). *Light alloys ; metallurgy of light metals* (First). London: Edward Arnold Ltd (pp 16 – 23).

Thornton, K., Ågren, J., & Voorhees, P. W. (2003). Modelling the evolution of phase boundaries in solids at the meso- and nano-scales. *Acta Materialia*, *51*(19), 5675–5710. https://doi.org/10.1016/j.actamat.2003.08.008

Vermolen, F. J., Vuik, C., Javierre, E., & Van Der Zwaag, S. (2005). Review on some Stefan problems for particle dissolution in solid metallic alloys. *Nonlinear Analysis: Modelling and Control*, *10*(3), 257–292. https://doi.org/http://www.lana.lt/journal/18/Vermolen.pdf

Vermolen, F. J., Vuik, C., & van der Zwaag, S. (2003). Particle dissolution and cross-diffusion in multi-component alloys. *Materials Science and Engineering A*, *347*(1–2), 265–279. https://doi.org/10.1016/S0921-5093(02)00615-9

Williams, S. W., Martina, F., Addison, A. C., Ding, J., Pardal, G., & Colegrove, P. (2015). Wire+arc additive manufacturing. *Materials Science and Technology*, 1743284715Y.000. https://doi.org/10.1179/1743284715Y.0000000073

Zhu, J. Z., Wang, T., Zhou, S. H., Liu, Z. K., & Chen, L. Q. (2004). Quantitative interface models for simulating microstructure evolution. *Acta Materialia*, *52*, 833–840. https://doi.org/10.1016/j.actamat.2003.10.017